Applied Catalysis B: Environmental 140–141 (2013) 98–107

Contents lists available at SciVerse ScienceDirect

Applied Catalysis B: Environmental

journal homepage: www.elsevier.com/locate/apcatb

High-throughput screening of monometallic catalysts for aqueous-phase hydrogenation of biomass-derived oxygenates

Jechan Lee[a,1], Ye Xu[b], George W. Huber[a,*,1]

[a] Department of Chemical Engineering, University of Massachusetts Amherst, 686 North Pleasant Street, Amherst, Massachusetts 01003, USA
[b] Center for Nanophase Materials Sciences, Oak Ridge National Laboratory, Oak Ridge, Tennessee 37831, USA

ARTICLE INFO

Article history:
Received 19 January 2013
Received in revised form 16 March 2013
Accepted 19 March 2013
Available online 26 March 2013

Keywords:
Aqueous-phase hydrogenation
Aqueous-phase hydrogenolysis
Binding energy
Biomass conversion
Heterogeneous catalysts
High-throughput

ABSTRACT

The initial reaction rates on a per site basis for aqueous-phase hydrogenation (APH) of different oxygenated compounds: including acetaldehyde, propanal, acetone, xylose, furfural, and furfuryl alcohol and aqueous-phase hydrogenolysis of tetrahydrofurfuryl alcohol (THFA) and xylitol were measured over various alumina-supported monometallic catalysts (Pd, Pt, Ru, Rh, Ni, and Co) in a high-throughput reactor. These oxygenated compounds have the same functionality that is found in aqueous solutions derived from biomass including pyrolysis oils and aqueous hydrolysis solutions. The initial rate of APH of the different carbonyls groups was dependent on the functionality of the feed molecule and catalyst used. Ru was the most active metal for APH of acetaldehyde, propanal, acetone, and xylose. Pd was the most active metal for APH of furfural and furfuryl alcohol. Only Pt and Ni catalysts were able to produce 1,2-pentanediol and 1,5-pentanediol from aqueous-phase hydrogenolysis of THFA. Ru was active for conversion of THFA but only made coke. The initial activity for aqueous-phase hydrogenolysis of xylitol decreased in the order of Ru > Co > Pt > Ni ≥ Pd. The initial rates of APH of carbonyl groups (C=O bond) measured in this study decreased in the order: hydrogenation of acetone > hydrogenation of acetaldehyde and propanal > hydrogenation of xylose > hydrogenation of furfural. The initial rates of aqueous-phase hydrogenolysis of THFA and xylitol were much lower than the initial rate for APH of C=O and C=C bonds.

1. Introduction

Aqueous-phase hydrogenation (APH) reactions are commonly used for conversion of biomass into different fuels and chemicals. For example, APH is a critical part of aqueous-phase processing (APP) [1–6] for the conversion of sugars into light and large alkanes, including the production of hexane from sorbitol [2] and the conversion of glucose into C9, C12, and C15 alkanes [1]. Hydrodeoxygenation (HDO) is an important technology for the upgrading of bio-oils and vegetable oils into fuels [7–11]. APH is a critical step in aqueous-phase hydrodeoxygenation (APHDO) where hydrogen is added to biomass derived molecules to hydrogenate C=O and C=C bonds. There are several types of functionalities that are hydrogenated during APH of biomass. This includes the hydrogenation of C=O bonds, C=C bonds, C—O—C bonds, and organic acids. The molecules also may have other functional groups, like hydroxyl or furan rings, that impact the rate of hydrogenation by steric factors. It would be highly desirable to understand how the reaction rates for APH of these different functionalities changes with different catalyst surfaces.

In this study, we used eight different molecules, including acetaldehyde, propanal, acetone, xylose, furfural, furfuryl alcohol, THFA, and xylitol, as biomass-derived model compounds for aqueous-phase hydrogenation and hydrogenolysis. These molecules have the same functionalities that are present in the aqueous fractions of biomass-derived feedstocks like pyrolysis oils and hydrolysis solutions. Polyols such as xylitol and sorbitol can be produced from lignocellulosic biomass [12,13]. A large variety of alcohols, aldehydes, ketones, and furans are commonly found in bio-oil produced from fast pyrolysis of biomass [14]. Alcohols, ketones and tetrahydrofurans (THFs) can also be produced from HDO of polyol [15].

There have been many previous studies on the hydrogenation of different biomass-derived compounds over heterogeneous catalysts [16–26]. For example, Olcay et al. previously studied APH of acetic acid over a series of different metal catalysts [18]. Olcay et al. concluded that Ru is the most active metal, on a per site basis, for the conversion of acetic acid and the most selective

* Corresponding author at: Department of Chemical and Biological Engineering, University of Wisconsin-Madison, 1415 Engineering Drive, Madison, Wisconsin 53706, USA. Tel.: +1 608 263 0346.
E-mail address: huber@engr.wisc.edu (G.W. Huber).
[1] Present address: Department of Chemical and Biological Engineering, University of Wisconsin-Madison, 1415 Engineering Drive, Madison, Wisconsin 53706, USA.

0926-3373/$ – see front matter © 2013 Elsevier B.V. All rights reserved.
http://dx.doi.org/10.1016/j.apcatb.2013.03.031

toward ethanol production. The rate of catalyst activity decreased as Ru > Rh ~ Pt > Pd ~ Ir > Ni > Cu. Narayanan et al. tested alumina supported Ni, Co, and Fe catalysts for the vapor phase hydrogenation of acetone, and concluded that the activity decreased as Ni > Co > Fe [27]. A different study indicated that the activity for xylose hydrogenation in aqueous-phase followed the order of Ru > Rh > Pd [28]. Another study compared five different metal catalysts (Pt, Ir, Ru, Ni, and Co) for the vapor phase hydrogenation of acrolein, concluding that Pt and Ru had faster reaction rates for acrolein hydrogenation under vapor phase than Ir, Ni, and Co [29]. In spite of the numerous studies that have been done on hydrogenation of different biomass functionalities, there has been no systematic study for APH of different biomass-derived feedstocks containing different functionalities over a range of catalysts. It would be highly desirable to systematically understand APH activity of different biomass derived molecules over different metal surfaces.

High-throughput techniques have been developed to rapidly screen large amounts of catalytic material [30–37]. The advantage of high-throughput catalytic studies is that large data bases can be rapidly screened. However, high-throughput methods do not always provide the comprehensive information provided by more in-depth studies about the catalysts like deactivation rates. Nevertheless, high-throughput studies have lead to the development of more efficient catalysts for many processes including the aqueous phase reforming of biomass [38], oxidation of propane [39], and hydrogen evolution reactions [40]. The objective of this study is to measure the initial activity of different supported monometallic catalysts including Pd, Pt, Ru, Rh, Ni, and Co for APH of different carbonyl groups (acetaldehyde, propanal, acetone, xylose, and furfural), APH of C=C bonds (furfuryl alcohol), and aqueous-phase hydrogenolysis of C—O—C bonds (THFA) and C—C bonds (xylitol) using a high-throughput reactor (HTR). We also compare the intrinsic reactivity for APH of the metals with the binding energy of atomic C and O, the two key elements involved in the bonding of the surface intermediates with the metals. The binding energies of atomic C and O are calculated using density functional theory (DFT), in an attempt to identify the relationship between the binding energy and the APH activity.

2. Experimental

2.1. Catalyst preparation

Monometallic catalysts with different metal loadings were prepared by incipient wetness impregnation with aqueous solutions of the following metal precursors: $[Pd(NH_3)_4](NO_3)_2$, $[Pt(NH_3)_4](NO_3)_2$, $Ru(NO)(NO_3)_3$, $Ni(NO_3)_2{\cdot}6H_2O$, and $Co(NO_3)_2{\cdot}6H_2O$ (Strem Chemicals Inc.). A 5 wt% Rh/Al_2O_3 catalyst was directly purchased from Strem Chemicals Inc. γ-alumina (γ-Al_2O_3, surface area: 142 m^2/g) was used as the support. The support was formed from Boehmite (Catapal® A Alumina, Sasol North America Inc.) pretreated at 873 K for 4 h. After impregnation catalysts were dried at 373 K for 12 h. The Pd and Pt catalysts were calcined at 523 K (ramping rate: 20 K/min) in stagnant air. The Ni and Co catalysts were calcined at 823 K (ramping rate: 20 K/min) for 4 hours in stagnant air. The Pd, Pt and Ru catalysts were pre-reduced individually under H_2 flow (50 ml/min, 99.99% Airgas) at 573 K (ramping rate: 1 K/min) for 2 h. The Ni and Co catalysts were also pre-reduced individually at 673 K (ramping rate: 1 K/min) for 4 h, the same temperature that was used elsewhere to reduce Ni and Co supported catalysts [41,42]. All prepared monometallic catalysts were stored in a glove box after pre-reduction to avoid oxidation.

2.2. Catalyst characterization

Hydrogen chemisorption was carried out in Quantachrome Autosorb iQ Automated Gas Sorption system according to the method of Shen et al. [43]. The metal dispersion (D) of Pd, Pt, Ru, and Rh, defined as the fraction of the total number of metal atoms on the support surface to the total number of metal atoms in the bulk sample [43], and hydrogen uptake of Ni and Co were obtained from the chemisorption results. Before chemisorption, all catalysts were reduced in situ under H_2 flow up to 573 K (Pd, Pt, Ru, and Rh) and 673 K (Ni and Co) with a heating rate 1 K/min, held for 2 hours, purged with He for 2 hours, evacuated for 140 min, and cooled to room temperature. Hydrogen was dosed on the catalyst until the equilibrium pressure was 560 mmHg. The hydrogen was then evacuated at room temperature, and again hydrogen was then reintroduced to determine the amount of weakly adsorbed hydrogen. The amount of strongly adsorbed hydrogen was determined by subtracting the second isotherm from the first one.

2.3. Catalytic activity measurements

High-throughput studies, which test multiple reactions in a single reactor system, have been used to rapidly screen a number of catalysts [44–49]. In this study, we used a high-throughput reactor (HTR) manufactured by HEL Group (Model # CAT24) to rapidly screen monometallic catalysts for different APH reactions. This reactor consisted of 24 wells (a well where a glass tube reactor put in) machined into a cylindrical stainless steel high pressure chamber, which allows catalysts to be tested 24 times faster than in a traditional batch reactor. Inside the chamber, stainless steel cooling tips were inserted into the top of each well, preventing the mixing of vapor between glass tube reactors. The system temperature, pressure, gas flow rate, and stirring speed (rpm) were controlled and monitored through WinIso E670 system software.

Prior to the reaction, catalysts were loaded into glass tubes and placed in the HTR in the glove box. This system was then treated under H_2 flow (100 ml/min, 99.99% Airgas) at 473 K (ramping rate: 1 K/min) for 12 h. Each catalyst was typically put into two different random wells to measure the effect of cross-talk between wells. There was rarely cross-talk between wells. Catalysts which were put into the two different random wells had similar results with a standard deviation of the measured TOF of around 7%. After additional treatment with H_2, magnetic stir bars were placed and 2 ml of an aqueous feedstock solution was added to each vial with a micropipette in the glove box. The HTR was then put on a heater, connected to the control system and the HTR was pressurized to 650 psia with H_2. Next, the HTR was heated to the reaction temperature at a rate of 20 K/min. More H_2 was introduced to maintain the final pressure at 800 psia. The heat up time for a typical experiment was 5–13 min. The reaction time was between 30 and 360 min indicating that minimal reactions occur during temperature ramp up.

A stirring speed of 800 rpm was used during a reaction. Experiments of THFA hydrogenolysis at 523 K (the highest temperature used in this study) with the stirring speed of 500 rpm and 800 rpm showed no change in conversion or selectivity. This indicates there was no external mass transfer limitation in this study. Once a reaction set finished, the HTR was removed from the heater and cooled down in an ice bath at a rate of around 14 K/min. After reaching room temperature, the HTR was depressurized to atmospheric pressure, and samples in each well were taken by a 3 mL syringe and filtered by a syringe filter (0.2 μm). The samples were analyzed by gas chromatograph (GC; Agilent 7890 A) using Rtx-VMS capillary column and a flame ionization detector (FID). A high performance liquid chromatography (HPLC; Shimadzu LC-20AT) with UV–vis (SPD-20AV) and RID (RID-10A) detectors was used to analyze sugars such as xylose and xylitol.

Table 1
Chemisorption data of catalysts used in this study.

Catalysts	H_2 uptake/μmol g^{-1}	Dispersion/%	Mean particle size[a]/nm
0.5 wt% Pd/Al_2O_3	12.4	52.6	2.1
1 wt% Pd/Al_2O_3	21.0	44.7	2.5
3 wt% Pd/Al_2O_3	58.1	41.2	2.7
0.5 wt% Pt/Al_2O_3	7.3	57.2	2.0
1 wt% Pt/Al_2O_3	14.0	54.4	2.1
3 wt% Pt/Al_2O_3	37.7	49.1	2.3
0.5 wt% Ru/Al_2O_3	3.6	14.7	8.8
1 wt% Ru/Al_2O_3	9.4	19.1	6.8
3 wt% Ru/Al_2O_3	34.3	23.1	5.6
5 wt% Rh/Al_2O_3	72.9	30.0	3.6
5 wt% Ni/Al_2O_3	10.0	–	–
10 wt% Ni/Al_2O_3	31.5	–	–
20 wt% Ni/Al_2O_3	84.7	–	–
5 wt% Co/Al_2O_3	6.2	–	–
10 wt% Co/Al_2O_3	8.6	–	–
20 wt% Co/Al_2O_3	18.1	–	–

[a] Mean particle size = $6(v_m/a_m)/D$ where v_m = volume occupied by an atom in bulk metal, a_m = area occupied by a surface atom, D = dispersion [59]. The values of v_m and a_m of metals are presented in supplementary data. The structure of metals is assumed to be fcc (Pd, Pt, Rh, and Ni) and hcp (Ru and Co) [59].

In this study, we measured the initial turnover frequency (TOF) of each metal catalyst at conversions of less than 31% to compare the initial activity of monometallic catalysts for APH of different functionalities. Reaction times were varied to obtain the conversions less than 31% (see Table S2). We tested each catalyst at least three times, and we report here the average value of the initial TOF and the standard deviation of our measurements (see Table 2). The standard deviation of the initial TOF were typically within 15% of the average initial TOF value indicating that there was little variability in our measurements. The initial TOF of each reaction was calculated by the equations:

$$\text{TOF} = \frac{(\text{moles of product})}{\{(\text{moles of metal in catalyst}) \times (\text{dispersion}) \times (\text{reaction time})\}}$$

The carbon balance was obtained by measuring the carbon in the liquid phase by GC-FID and HPLC, calculated by the equation:

$$\text{Carbon balance (\%)} = 100 \times \frac{(\text{moles carbon out (all products and reactants)})}{(\text{moles of carbon in})}$$

2.4. Computational methods

Periodic density functional theory (DFT) calculations were performed in the generalized gradient approximation (GGA-PBE) [50] using the Vienna Ab initio Simulation Package (VASP) [51–53]. The core electrons were described by the projector augmented wave method [54], and the Kohn–Sham valence states were expanded in a plane wave basis set up to a kinetic energy of 400 eV. A first-order Methfessel–Paxton scheme was used for the smearing of electronic states with a smearing temperature of 0.1. All total energies were extrapolated to 0 K.

The equilibrium PBE bulk lattice constants were calculated to be 2.49/4.04 (Co), 3.52 (Ni), 2.73/4.30 (Ru), 3.84 (Rh), 3.95 (Pd), and 3.98 (Pt) Å, in good agreement with the experimental values [55] (2.51/4.07 (Co), 3.52 (Ni), 2.70/4.27 (Ru), 3.80 (Rh), 3.89 (Pd), and 3.92 (Pt) Å). Extended metal surfaces were represented by slabs exposing the thermodynamically most stable (1 1 1) facet of Ni, Rh, Pd, and Pt and (0001) facet of Co and Ru. Each slab was constructed from a (3 × 3) surface unit cell (corresponding to 1/9 ML coverage of each adsorbate) with four layers of metal atoms and was separated from neighbouring slabs in the z direction by seven layers equivalent of vacuum. The top two layers were relaxed and the remaining two held fixed at bulk positions. The surface Brillouin zone was sampled with a 5 × 5 × 1 Monkhorst–Pack k-point mesh. The choice of slab thickness and k-point sampling density were verified to converge the total energy to within 0.05 eV. Calculations for Co and Ni were spin-polarized.

Atomic adsorption was modeled on one side of the slab only with dipole decoupling [56]. The binding energy (BE) of an adatom was calculated as $\text{BE} = E_{\text{ads}} - E_{\text{clean}} - E_{\text{gas}}$, where E_{ads}, E_{clean} and E_{gas} are the total energies of the slab with the adsorbate on it, the metal slab without the adsorbed atom, and the neutral atom in the gas phase, respectively.

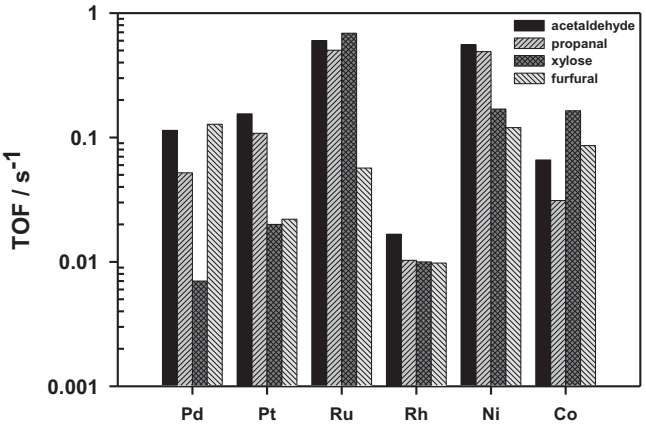

Fig. 1. Initial TOF for APH of aldehydes over monometallic catalysts at 373 K with 5 wt% (acetaldehyde, propanal, xylose) and 4.8 wt% (furfural) aqueous solution as the feed.

3. Results

3.1. Catalyst characterization

Table 1 summarizes the H_2 chemisorption data obtained on alumina-supported monometallic catalysts with varying metal loadings. We used this data to estimate the dispersion and mean particle sizes of the precious metal catalysts. We do not estimate the dispersion of the Ni and Co catalysts because we did not measure the degree of reducibility of these metals. Ni and Co catalysts are known to form metal-aluminate phases that are difficult to reduce [57]. The H_2 chemisorption data measured in this study is consistent with the values reported in previous studies. For example, the value of H_2 uptake of the 1 wt% Pd catalyst agrees well with the work of Wang et al. who also prepared a Pd/Al_2O_3 catalyst [58].

3.2. Aqueous-phase hydrogenation of C=O and C=C functionalities

Table 2 summarizes the initial TOFs of different hydrogenation reactions in the aqueous phase over the different monometallic catalysts. The conversions, reaction times, and carbon balances are provided in Tables S2 and S3. There is no clear trend of the initial activity as a function of metal loading in the limited range of particle sizes used in this study. The results of the initial TOF for APH of the four different aldehydes are shown in Fig. 1. This figure only shows the most active of each of the monometallic catalysts series. Only ethanol was observed for the APH of acetaldehyde. 1-Propanol was the only product observed from APH of propanal. The initial TOF for APH of acetaldehyde and propanal decreased in the order: Ru ~ Ni > Pt > Pd > Co > Rh. The 3 wt% Ru catalyst was the most active catalyst for APH of acetaldehyde and propanal. The Pt catalysts were more active than the Pd catalysts; for instance, the initial TOF of the

Table 2
Initial TOF (s^{-1}) for aqueous-phase hydrogenation of different feedstocks over monometallic catalysts.

Functionality Temperature Feedstock	C=O bond 373 K acetaldehyde	C=O bond 373 K propanal	C=O bond 373 K acetone	C=O bond 373 K xylose	C=O bond 373 K furfural	C=C bond 353 K furfuryl alcohol
0.5 wt% Pd/Al_2O_3	0.114 (±0.013)	0.045 (±0.005)	0.026 (±0.003)	0.007 (±0.001)	0.043 (±0.004)	0.076 (±0.005)
1 wt% Pd/Al_2O_3	0.100 (±0.011)	0.052 (±0.005)	0.033 (±0.004)	0.006 (±0.001)	0.092 (±0.005)	0.068 (±0.006)
3 wt% Pd/Al_2O_3	0.080 (±0.007)	0.028 (±0.0031)	0.030 (±0.004)	0.004 (±0.0004)	0.128 (±0.007)	0.037 (±0.002)
0.5 wt% Pt/Al_2O_3	0.149 (±0.014)	0.094 (±0.018)	0.240 (±0.029)	0.019 (±0.002)	0.022 (±0.001)	0.006 (±0.0007)
1 wt% Pt/Al_2O_3	0.155 (±0.011)	0.108 (±0.016)	0.203 (±0.024)	0.020 (±0.003)	0.016 (±0.001)	0.004 (±0.0003)
3 wt% Pt/Al_2O_3	0.143 (±0.009)	0.089 (±0.012)	0.486 (±0.067)	0.014 (±0.002)	0.014 (±0.001)	0.003 (±0.0001)
0.5 wt% Ru/Al_2O_3	0.340 (±0.036)	0.409 (±0.038)	1.372 (±0.101)	0.214 (±0.023)	0	0
1 wt% Ru/Al_2O_3	0.436 (±0.046)	0.369 (±0.027)	4.737 (±0.269)	0.295 (±0.031)	0	0.018 (±0.002)
3 wt% Ru/Al_2O_3	0.602 (±0.012)	0.503 (±0.044)	4.701 (±0.214)	0.688 (±0.032)	0.057 (±0.006)	0.040 (±0.004)
5 wt% Rh/Al_2O_3	0.017 (±0.002)	0.010 (±0.001)	0.558 (±0.053)	0.010 (±0.001)	0.010 (±0.001)	0.005 (±0.0006)
5 wt% Ni/Al_2O_3	0.194 (±0.010)	0.184 (±0.024)	0.427 (±0.050)	0.149 (±0.016)	0.107 (±0.006)	0.056 (±0.006)
10 wt% Ni/Al_2O_3	0.557 (±0.023)	0.490 (±0.033)	0.592 (±0.042)	0.169 (±0.019)	0.120 (±0.008)	0.062 (±0.005)
20 wt% Ni/Al_2O_3	0.301 (±0.022)	0.228 (±0.031)	0.311 (±0.034)	0.093 (±0.009)	0.084 (±0.006)	0.024 (±0.002)
5 wt% Co/Al_2O_3	0.066 (±0.007)	0	0.368 (±0.037)	0.164 (±0.008)	0.086 (±0.005)	0
10 wt% Co/Al_2O_3	0	0	0.192 (±0.021)	0.041 (±0.002)	0.012 (±0.001)	0
20 wt% Co/Al_2O_3	0.019 (±0.002)	0.031 (±0.002)	0.065 (±0.003)	0.054 (±0.012)	0.022 (±0.002)	0

3 wt% Pt catalyst was 79% higher than the initial TOF of the 3 wt% Pd catalyst for APH of acetaldehyde. The 5 wt% Rh catalyst had the lowest initial activity for APH of acetaldehyde and propanal.

Xylitol was the only product produced from APH of xylose at 373 K. The initial TOF for APH of xylose decreased in the order: Ru > Ni ~ Co > Pt > Rh ~ Pd (See Fig. 1). This result is consistent with the work of Wisniak et al. who concluded that the rate of xylose hydrogenation decreased according to the order Ru > Ni > Rh > Pd [28,60]. Yadav et al. also concluded that supported Ru catalysts were more selective to xylitol than Raney Ni catalyst for the hydrogenation of xylose [61]. The 3 wt% Ru catalyst had the highest initial activity for APH of xylose with an initial TOF of 0.688 s^{-1}. The second most active metals were the 10 wt% Ni catalyst (0.169 s^{-1}) and the 5 wt% Co catalyst (0.164 s^{-1}). The 3 wt% Pd catalyst had the lowest initial TOF (0.004 s^{-1}) for APH of xylose. The 3 wt% Pt catalyst was 40% more active than the 5 wt% Rh catalyst. The major differences between APH of acetaldehyde, propanal, and xylose are: 1) the Pd catalysts had much lower initial activity for APH of xylose than for APH of acetaldehyde and propanal; and 2) the Co catalysts had even higher initial activity for APH of xylose than for APH of acetaldehyde and propanal.

Furfuryl alcohol was the only product detected on Pt, Ru, Rh, and Co for APH of furfural at 373 K. THFA was further produced over the Pd and Ni catalysts with a prodcut distribution (100 × (moles of THFA)/(moles of furfuryl alcohol + moles of THFA)) of 9.5% and 8.4% respectively. The initial activity for APH of furfural decreased in the order: Pd ~ Ni > Co > Ru > Pt > Rh. The 3 wt% Pd catalyst had the highest initial activity (0.128 s^{-1}) for APH of furfural. The 5 wt% Rh catalyst had the lowest initial activity (0.010 s^{-1}) for APH of furfural. The formation of THFA over Pd and Ni from APH of furfural indicates that they are also active in hydrogenating the C=C bond in the furan ring, which is consistent with the data discussed later on in this paper.

The major differences between the initial activity for APH of furfural (i.e. furanic aldehyde) and APH of acetaldehyde and propanal (i.e. non-furanic aldehyde) are: 1) Among the different metals Pd has a very high initial activity for APH of furfural, but has a very low initial activity for APH of acetaldehyde and propanal; 2) Co is more active for APH of furfural than for APH of acetaldehyde and propanal; 3) Ru is more active for APH of acetaldehyde and propanal than for APH of furfural.

In addition, the initial TOF of the 3 wt% Pd catalyst for APH of furfural was lower than the initial TOF of the 3 wt% Ru catalyst for APH of acetaldehyde and propanal. This indicates that the initial rate of hydrogenation of non-furanic aldehydes is faster than the initial rate of hydrogenation of furanic aldehydes in the aqueous phase.

We also tested APH of acetone, where the ketone was hydrogenated. Isopropyl alcohol was the only product detected on all the catalysts from APH of acetone. The comparison of the initial TOF for APH of propanal and acetone is shown in Fig. 2. The initial TOF for APH of acetone decreased in the order: Ru > Ni ~ Rh > Pt > Co > Pd, compared to the order of initial TOF for APH of propanal: Ru ~ Ni > Pt > Pd > Co > Rh. The initial rate of APH of acetone was faster than the initial rate of APH of the aldehydes for all catalysts except for Pd. For example, over the 3 wt% Ru catalyst, the initial TOF for APH of acetone was 8.3 times higher than the initial TOF for APH of propanal. Zheng et al. showed that acetaldehyde hydrogenation occurred more slowly than acetone hydrogenation in the gas phase on Pt and Co catalysts [62]. There was a large difference of the initial TOF of more than two orders of magnitude between propanal and acetone with Rh. This is consistent with the work of van Druten and Ponec who reported that a supported Rh catalyst showed much higher conversion for acetone hydrogenation than propanal hydrogenation in the gas phase [63].

The initial TOF of different metals for APH of furfuryl alcohol, which involves the hydrogenation of C=C bonds, is shown in Fig. 3. This reaction was done at 20 K lower in temperature than the APH of aldehydes for the purpose of obtaining good carbon balances (more than 90%, see Table S3). THFA was the only product detected in these experiments. The initial activity for THFA production by APH of furfuryl alcohol decreased in the order: Pd > Ni > Ru > Pt > Rh ≫ Co. Sitthisa and Resasco showed that Pd and Ni catalysts were active for the production of THFA from furfuryl

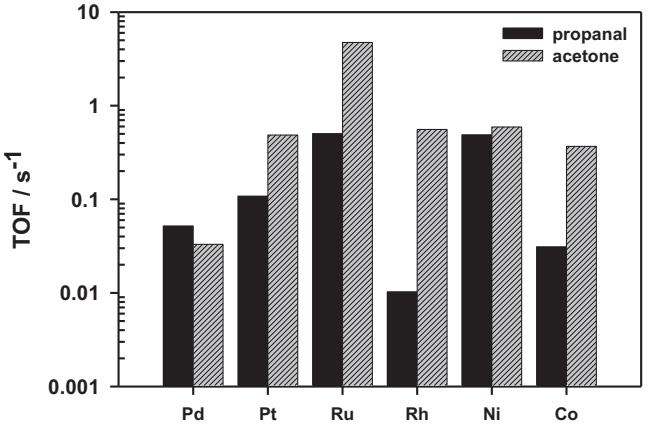

Fig. 2. Initial TOF for APH of propanal and acetone at 373 K with 5 wt% aqueous solution as the feed.

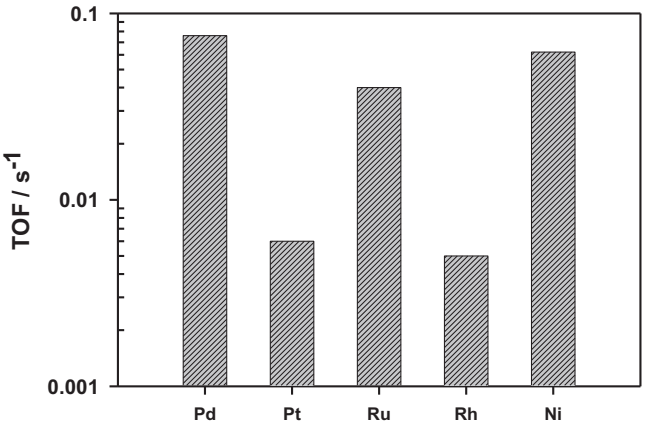

Fig. 3. Initial TOF for APH of furfuryl alcohol over monometallic catalysts at 353 K with 4.8 wt% furfuryl alcohol solution as the feed.

alcohol [64]. The Co catalysts were inactive for APH of furfuryl alcohol at 353 K in this study. Pt and Rh showed very slow initial rates of APH of furfuryl alcohol within the range of TOFs from 0.003 to 0.006 s^{-1}.

3.3. Aqueous-phase hydrogenolysis of C—O—C and C—C bond

Aqueous-phase hydrogenolysis of THFA was studied to measure the initial rate of C—O—C bond hydrogenolysis (Table 3). We used a temperature of 523 K for aqueous-phase hydrogenolysis of THFA because no 1,2-pentanediol or 1,5-pentanediol was observed at temperatures below 523 K. THF and 1-butanol were detected from THFA conversion over all monometallic catalysts tested in this study. However, only Pt and Ni catalysts produced 1,2-pentanediol or 1,5-pentanediol via breaking the C—O bond of THFA. Sitthisa and Resasco showed that C—O bond cleavage occurred on Ni catalysts for THF hydrogenolysis to butanol [64].

With the Ru catalysts only a small amount of liquid products remained in the vial after reaction with carbon balances less than 1% for aqueous-phase hydrogenolysis of THFA. This is most probably due to polymerization reactions that form coke on the Ru surface. Ni was more active than Pt for aqueous-phase hydrogenolysis of THFA.

The initial rate of aqueous-phase hydrogenolysis of THFA was a lot slower than the initial rate of APH of carbonyl groups even though aqueous-phase hydrogenolysis of THFA was carried out at 150–170 K higher temperature. For instance, the initial TOF of 3 wt% Pt for aqueous-phase hydrogenation of acetaldehyde at 373 K was 46.7 times higher than the initial TOF of 3 wt% Pt for aqueous-phase hydrogenolysis of THFA at 523 K.

Pt and Ni produced different products from aqueous-phase hydrogenolysis of THFA. Pt and Ni produced 1,2-pentanediol and 1,5-pentanediol respectively suggesting they each cleave the C—O—C bond differently.

Aqueous-phase hydrogenolysis of xylitol was carried out at 473 K as a model reaction for C—C bond cleavage. Table 4 shows the initial activity and selectivity for xylitol hydrogenolysis in the aqueous phase. The initial activity for aqueous-phase hydrogenolysis of xylitol decreased as: Ru > Co > Pt > Ni > Pd. The main products, with the Pt, Ru, Ni and Co catalysts, were ethylene glycol and propylene glycol. Propylene glycol was the only observed product

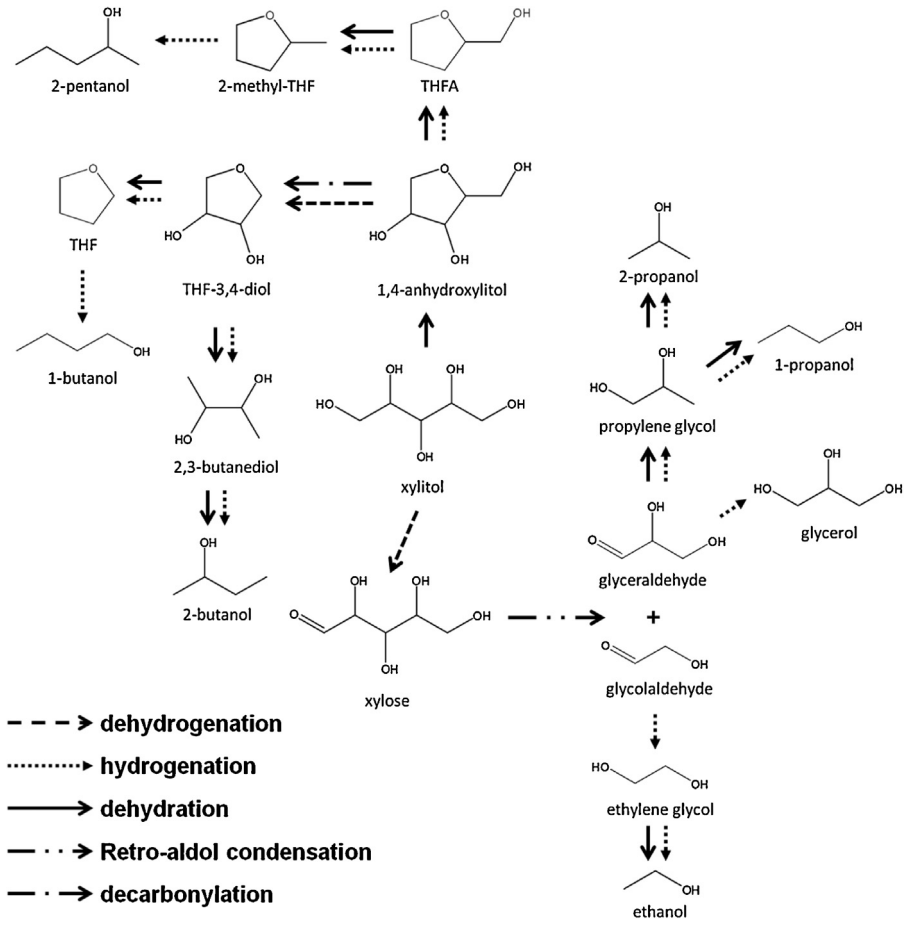

Fig. 4. Proposed reaction pathways for aqueous-phase hydrogenolysis of xylitol at 473 K with 5 wt% xylitol solution as the feed.

Table 3
Initial TOF and selectivity for aqueous-phase hydrogenolysis of THFA over monometallic catalysts at 523 K with 5 wt% THFA solution as the feed.

Catalysts	TOF[a]/s^{-1}	Conversion[b]/%	Carbon balance/%	Selectivity[c]/%			
				THF	1-butanol	1,2-pentanediol	1,5-pentanediol
3 wt% Pt/Al_2O_3	0.003	9.3	95.9	4.6	12.4	38.9	0
5 wt% Ni/Al_2O_3	0.003	8.3	93.5	4.2	8.0	0	9.7
10 wt% Ni/Al_2O_3	0.006	14.3	93.1	2.6	6.7	0	42.4
20 wt% Ni/Al_2O_3	0.004	17.3	95.0	2.2	9.9	0	59.2

[a] TOF of THFA to pentanediols.
[b] Conversion (%) = 100 × (moles of THFA converted)/(moles of THFA in feed).
[c] Selectivity (%) = 100 × (moles of carbon in product)/(moles of carbon in THFA converted).

with the 3 wt% Pd catalyst; however, the 3 wt% Pd catalyst had an extremely slow initial reaction rate. Small amounts of glycerol were detected with Ru catalysts. Only ethylene glycol, propylene glycol and ethanol were detected with the Co catalysts.

Fig. 4 shows the reaction pathways that we propose for aqueous-phase hydrogenolysis of xylitol. Our previous study showed that decarbonylation, dehydrogenation, hydrogenation and retro-aldol condensation reactions occur on metal sites, whereas dehydration reaction occurs on acid sites [65]. Xylitol can undergo two different parallel reactions. One of these reactions involves an initial dehydration step to 1,4-anhydroxylitol, similar to the reaction pathway for APHDO of sorbitol shown in our previous study [65]. The 1,4-anhydroxylitol can undergo further dehydration and hydrogenation to produce THFA. The THFA can yield 2-methyltetrahydrofuran by dehydration and hydrogenation. The 2-methyltetrahydrofuran can react with H_2 further to form 2-pentanol. 2-Pentanol is probably produced by hydrogenolysis of C—O—C bond in 2-methyltetrahydrofuran on Pt and Ru surfaces only, which is consistent with the results from THFA hydrogenolysis in this study. The 1,4-anhydoxylitol is also able to undergo decarbonylation to tetrahydrofuran-3,4-diol from which 2,3-butanediol and tetrahydrofuran (THF) can be produced further by dehydration and hydrogenation. 2-butanol and 1-butanol are possibly made from 2,3-butanediol and THF by undergoing dehydration and hydrogenation, respectively. C_1–C_3 compounds are produced mainly via retro-aldol condensation, also described in the literature [66]. Xylitol converts to xylose via dehydrogenation, and the aldehyde, xylose, can undergo retro-aldol condensation to produce glycolaldehyde and glyceraldehyde. The glycolaldehyde then reacts with H_2 to form ethylene glycol, and the glyceraldehyde further makes propylene glycol via dehydration and hydrogenation.

4. Discussion

4.1. Catalytic activity

Table 5 summarizes the results of this study and compares the results with previous studies done for hydrogenation reactions [18,27,28,60,62,66–68]. Generally, the order of catalytic activity from this study is consistent with previous studies. Ru is always the most active monometallic catalyst for aqueous-phase (or liquid-phase) hydrogenation of non-furanic carbonyl groups. We have previously shown that Ru is the most active monometallic catalyst for APH of acetic acid to ethanol in a continuous-flow reactor [18]. Ru is also the most active metal for hydrogenolysis of polyol under neutral conditions [66,67]. Pd is the most active metal for APH of carbonyl groups that contain furan rings in this study. Previous studies also observed that Pd is an effective catalyst for furfural hydrogenation to the corresponding alcohol at low temperatures [69,70].

The reaction rate for hydrogenation of different biomass feedstocks is dependent on steric effects of other functionalities on the molecule. For example, the rate of APH of non-furanic aldehydes (i.e. acetaldehyde, propanal) is faster than the rate of APH of furanic aldehyde (i.e. furfural). Thus, the furan ring inhibits the rate of hydrogenation of carbonyl groups. The rate of xylose hydrogenation is also slower than the rate of hydrogenation of acetaldehyde and propanal (with the exception of the 3 wt% Ru catalyst and the Co catalysts). This also suggests that the five hydroxyl groups on xylose cause steric hindrance which inhibits the rate of xylose hydrogenation. Previous studies also showed that steric hindrance of hydroxyl groups can decrease the rate of hydrogenation [71]. The rate of hydrogenation of ketone (i.e. acetone) is much faster than hydrogenation of aldehydes (i.e. acetaldehyde and propanal) for all catalysts tested in this study. A possible reason why acetone hydrogenation is much faster than propanal hydrogenation under the same reaction conditions is that propanal is adsorbed more strongly than acetone [63]. Furthermore, tetrahydrofuran (THF) ring opening reactions only occur on Pt and Ni (and potentially Ru). This is probably because the interaction between Ni and the THF ring is so strong that it weakens the C—O bond enough to open the THF ring [64].

We have not used the high-throughput technique in this paper to study catalyst deactivation even though it is well known that catalyst deactivation is known to occur under aqueous-phase conditions. In this study we assume that we are only measuring the initial catalytic activity. Catalyst deactivation for aqueous-phase reactions can occur by phase transformation of the metal oxide support [72,73], dissolution, sintering of the metal particles [38,74–76], and coke formation on the catalyst surface [77]. For example, Sievers and co-workers showed that under aqueous-phase conditions alumina undergoes a phase transformation from γ-alumina to hydrated boehmite accompanied with a loss of surface area [72]. Shabaker et al. found that alumina-supported Ni catalysts deactivated by sintering in the aqueous-phase [74].

4.2. Relation between TOF and binding energy of atomic C and O

The number of feeds and catalysts included in our study precludes a detailed examination of the reaction mechanism and theoretical prediction of catalytic activity for each compound on the different metals in this report. Some mechanistic insights, nonetheless, may be gleaned from an empirical combination of the experimentally measured catalytic activity and certain descriptions of the fundamental reactivity of the metals. We take the hydrogenation of acetaldehyde (CH_3CHO) as an example. If we limit ourselves to considering only the selective pathway(s) to ethanol, as is in line with the near-unity selectivity, then there are two alternative pathways, as distinguished by the intermediate involved (ethoxy (CH_3CH_2O) or 1-hydroxyethyl (CH_3CHOH)):

$$CH_3CHO + H \rightarrow CH_3CH_2O; \quad CH_3CH_2O + H \rightarrow CH_3CH_2OH, \text{ or}$$

$$CH_3CHO + H \rightarrow CH_3CHOH; \quad CH_3CHOH + H \rightarrow CH_3CH_2OH$$

The starting molecule, acetaldehyde, binds the metals weakly through the C=O group [18]. The intermediates are open-shell

Table 4
Initial TOF and selectivity for aqueous-phase hydrogenolysis of xylitol over monometallic catalysts at 473 K with 5 wt% xylitol solution as the feed.

Catalysts	TOF ($\times 10^{-3}$)[a]/s^{-1}	Conversion[b]/%	Carbon balance/%	Selectivity[c]/%									
				methanol	ethanol	ethylene glycol	propanol[d]	propylene glycol	glycerol	butanol[e]	butanediol[f]	2-pentanol	THFA
3 wt% Pd/Al_2O_3	0.3	9.5	90.9	0	0	0	0	3.4	0	0	0	0	0
0.5 wt% Pt/Al_2O_3	5.3	9.2	91.5	0	0	2.6	0	5.2	0	0	0	0	0
1 wt% Pt/Al_2O_3	3.3	8.3	92.6	0	1.9	3.1	1.8	3.5	0	0	0	0	0
3 wt% Pt/Al_2O_3	3.6	11.8	90.8	1.4	2.0	5.3	1.5	6.4	0	2.4	0	1.8	1.0
0.5 wt% Ru/Al_2O_3	28.3	8.3	93.2	1.4	2.7	6.3	2.1	4.5	0	0	1.6	0	0
1 wt% Ru/Al_2O_3	91.7	14.1	92.2	1.0	3.3	9.9	4.1	10.8	4.8	2.6	5.6	1.4	1.0
3 wt% Ru/Al_2O_3	48.3	16.4	92.4	0.9	4.0	3.2	7.2	13.6	4.0	5.3	13.5	2.2	0
10 wt% Ni/Al_2O_3	3.6	4.3	97.9	0	3.7	29.3	0	18.5	0	0	0	0	0
20 wt% Ni/Al_2O_3	1.9	8.9	94.1	2.5	2.3	16.3	0	9.1	0	0	1.8	0	1.5
5 wt% Co/Al_2O_3	24.2	8.3	94.6	0	2.0	16.6	0	16.1	0	0	0	0	0
10 wt% Co/Al_2O_3	13.3	10.0	92.3	0	2.2	10.3	0	10.5	0	0	0	0	0
20 wt% Co/Al_2O_3	4.4	7.1	94.3	0	3.0	9.1	0	7.7	0	0	0	0	0

[a] TOF = (sum of moles of carbon in product)/{(moles of metal in catalyst) × (dispersion) × (reaction time)}.
[b] Conversion (%) = 100 × (moles of xylitol converted)/(moles of xylitol in feed).
[c] Selectivity (%) = 100 × (moles of carbon in product)/(moles of carbon in xylitol converted).
[d] Propanol includes 1-propanol and 2-propanol.
[e] Butanol includes 1-butanol and 2-butanol.
[f] Butanediol includes 1,2-butanediol and 2,3-butanediol.

Fig. 5. Initial TOF for APH of (a) acetaldehyde and (b) furfural on the different metals plotted again the calculated binding energies of atomic C and O on the fcc(1 1 1) and hcp(0 0 0 1) facets of these metals.

species and therefore bind the metals strongly: Ethoxy binds the surface through the O atom, and 1-hydroxyethyl through the C atom that is adjacent to the O [18]. Thus it may be expected that the different affinities of the metals toward C and O are a factor in deciding which pathway is operative in acetaldehyde hydrogenation to ethanol. This is a general, qualitative way of stating that scaling relations exist between key transition states along the selective hydrogenation pathways and reactivity descriptors such as the binding energies of C- and O-binding surface intermediates, which in turn scale with the binding energies of atomic C and O [78,79], across a series of metals.

The initial TOF of APH of acetaldehyde and furfural are plotted against the DFT-calculated binding energies of atomic C and O on the various metals in Fig. 5. The contours are generated based on

Table 5
Hydrogenation of biomass-derived molecules on different monometallic catalysts.

Reaction	Phase	Feed/product	Reaction conditions	Activity measured on	The order of activity	Reference
hydrogenation	aqueous	acetaldehyde/ethanol	373 K, 800 psia, 5 wt% acetaldehyde solution	a per site basis with H_2 chemisorption	Ru ∼ Ni > Pt > Pd > Co > Rh	this study
hydrogenation	aqueous	acetaldehyde/ethanol	343 K, H_2/acetaldehyde = 4:1	a per site basis with CO chemisorption	Pt > Co	Zheng et al. [62]
hydrogenation	aqueous	propanal/1-propanol	373 K, 800 psia, 5 wt% propanal solution	a per site basis with H_2 chemisorption	Ru ∼ Ni > Pt > Pd > Co > Rh	this study
hydrogenation	aqueous	acetone/2-propanol	373 K, 800 psia, 5 wt% acetone solution	a per site basis with H_2 chemisorption	Ru > Ni ∼ Rh > Pt > Co > Pd	this study
hydrogenation	gas	acetone/2-propanol	308 K, H_2/acetone = 2:1	a per site basis with CO chemisorption	Pt > Co	Zheng et al. [62]
hydrogenation	gas	acetone/2-propanol	373–523 K, 4.5 cm^3 h^{-1} acetone feed rate	a per site basis with H_2 chemisorption	Ni > Co > Fe	Narayanan et al. [27]
hydrogenation	aqueous	xylose/xylitol	373 K, 800 psia, 5 wt% xylose solution	a per site basis with H_2 chemisorption	Ru > Ni ∼ Co > Pt > Rh ∼ Pd	this study
hydrogenation	liquid	xylose/xylitol	373–398 K, 200–800 psig	a total catalyst basis	Ru > Ni > Rh > Pd	Wisniak et al. [28,60]
hydrogenation	aqueous	furfural/furfuryl alcohol	373 K, 800 psia, 4.8 wt% furfural solution	a per site basis with H_2 chemisorption	Pd ∼ Ni > Co > Ru > Pt > Rh	this study
hydrogenation	aqueous	furfuryl alcohol/THFA	353 K, 800 psia, 4.8 wt% furfuryl alcohol solution	a per site basis with H_2 chemisorption	Pd > Ni > Ru > Rh ∼ Pt ≫ Co	this study
hydrogenation	aqueous	acetic acid/ethanol	383–563 K, 5.17 MPa (750 psi), 10 wt% acetic acid solution	a per site basis with H_2 chemisorption	Ru > Pt ∼ Rh > Pd ∼ Ir > Ni > Cu	Olcay et al. [18]
hydrogenolysis	aqueous	xylitol/glycol	473 K, 800 psia, 5 wt% xylitol solution	a per site basis with H_2 chemisorption	Ru > Co > Pt > Ni > Pd	this study
hydrogenolysis	aqueous	xylitol/glycol	473 K, 4.0 MPa (580 psi), 10 wt% xylitol solution	normalized per metal atom	Pt > Ru > Pd ∼ Rh (with base)	Sun et al. [66]
hydrogenolysis	aqueous	glycerol/glycol	473 K, 40 bar (580 psi), 1 wt% glycerol solution	a per site basis with H_2 chemisorption	Ru > Pt (with no base) Pt > Ru (with base)	Maris et al. [67]
reforming	aqueous	ethylene glycol	483 K, 22 bar (319 psi), 10 wt% ethylene glycol solution	a per site basis with CO chemisorption	Pt ∼ Ni > Ru > Rh ∼ Pd > Ir (in terms of CO_2 production)	Davda et al. [68]

Table 6
DFT-calculated binding energies of atomic C and O on the different metal surfaces.

Metal	E(C)/eV	E(O)/eV	Metal	E(C)/eV	E(O)/eV
Pd(1 1 1)	−7.03	−4.48	Pd(6 6 3)	−7.05	−4.47
Pt(1 1 1)	−7.15	−4.20	Pt(6 6 3)	−7.18	−4.33
Ru(0 0 0 1)	−7.63	−5.90	Ru(6 6 3)	−7.60	−6.21
Rh(1 1 1)	−7.26	−5.04	Rh(6 6 3)	−7.27	−5.19
Ni(1 1 1)	−6.80	−5.40	Ni(6 6 3)	−6.82	−5.59
Co(0 0 0 1)	−6.73	−5.58	Co(6 6 3)	−6.83	−5.90

The lowest binding energies for atomic C and O on the (0 0 0 1) facet of hcp metals, the (1 1 1) facet of fcc metals, and the upper terrace along the edge of the (6 6 3) facet of fcc metals are reported. For simplicity, the step edges of Ru and Co are also modeled by an fcc(6 6 3) facet. The preferred binding sites are: for C, fcc (Pd, Pt) and hcp (Rh, Ni) on fcc(1 1 1); hcp on hcp(0 0 0 1); f1 (Pd, Pt) and h2 (Rh, Ru, Ni, Co) on fcc(6 6 3); for O, fcc on fcc(1 1 1); hcp on hcp(0 0 0 1); f1 (Pd, Pt, Rh, Ni) and b1 (Ru and Co) on fcc(6 6 3). See Ref. [84] for site designations along the fcc(6 6 3) step edge.

triangulation. The initial activities over Pd, Pt, Ru (3 wt%), Rh, Ni, and Co (5 wt%), which are the most similar metal loadings tested in this study, were selected for the correlations. All other experimental parameters, including the aqueous phase, the hydrogen pressure, and the system temperature, were identical. The binding energies of the two atomic species are listed in Table 6. Carbon binds more strongly to Ru and Rh than the other metals we tested. Among the rest of the metals, Pt and Pd bind oxygen atom more weakly, being the nobler of the metals in this study. The binding energies calculated on both the close-packed facets ((1 1 1) for fcc metals and (0 0 0 1) for hcp metals) and step edges are included for comparison, but only those on the close-packed facets are used in Fig. 5. Low-coordination sites on metal surfaces such as step edges and defects can alter the activity of elementary bond-breaking/bond-forming steps compared to close-packed sites [80,81]. In a study of ethanol decomposition on transition metals, Ferrin et al. used the reaction energy of CO dissociation as the criterion and concluded that Cu, Pt, and Pd step edges likely remain open but Ir, Rh, and Ru step edges are poisoned by dissociation products such as atomic C and O [79]. Based on this argument Ni and Co step edges should also be poisoned [18], consistent with carbide formation due to CO and ethylene adsorption which is observed to occur along Ni steps but not on terraces [82,83]. Moreover, our recent theoretical study on methyl acetate reactivity on Pd surfaces [84] suggests that the enhancement of the activation of organic oxygenates is more pronounced on the upper terrace of a step edge. Therefore the binding energies at step edges in Table 6 are calculated on the upper terrace of a step edge. The C and O binding energies are only modestly more stable for Pt and Pd, so the topologies of the plots in Fig. 5 would not change appreciably. Overall we anticipate a lack of significant activity enhancement due to step edges, which is congruent with the lack of any observable particle size effect on the initial activity, as mentioned earlier. More experimental and theoretical work will be needed to identify the most active sites for APH of these organic molecules and provide a detailed understanding of the effect of low-coordination sites on the overall activity of APH of biomass-derived oxygenates.

The activity surfaces outlined by the contours in Fig. 5 have very different topologies. For APH of acetaldehyde, the gradients of the surface along the E(O) and E(C) axes are of similar magnitude. The highest activity occurs at Ru, from where the surface slopes down in both directions. For APH of furfural, on the other hand, the gradient is much larger along the E(C) axis than the E(O) axis, with the maximum occurring toward weaker binding energies of C, which is the opposite of APH of acetaldehyde. Comparing the two plots shows that APH of furfural is significantly more sensitive to the reactivity of the metal toward C than APH of acetaldehyde is. This suggests that whereas overall the affinity for C and O plays comparable roles

in APH of acetaldehyde across the different metals, the affinity for C plays a dominant role in controlling the activity of APH of furfural. This type of interpretation was recently borne out by a microkientic study of methanol dehydrogenation to formaldehyde, where the reaction proceeds through either an O—H or a C—H scission pathway on different metals, resulting in steepest gradient in TOFs vs. E(O) or E(C) respectively [85]. It appears logical to attribute the difference to the furan ring, although oxygenates containing conjugated rings may not interact with metal surfaces directly through the rings under conditions such as high surface coverage [86]. The exact mechanistic origin of this difference between APH of acetaldehyde and furfural cannot be revealed by this rudimentary approach and remains to be elucidated. Nonetheless, the empirical relations as evidenced in Fig. 5 provide an idea on whether the affinity for C or O has more influence on desired activity and may serve as a basic screening tool for metal catalyst composition.

5. Conclusions

The monometallic Ru catalysts were the most active catalysts for APH of the non-furanic carbonyl groups (including acetaldehyde, propanal, acetone, and xylose). The monometallic Pd catalysts showed the highest initial rate for APH of furfural and C=C bond in furfuryl alcohol. Co catalysts had no activity for APH of C=C bond in furfuryl alcohol. The initial TOF for APH of acetone was higher than the initial TOF for APH of acetaldehyde and propanal. The initial rate of APH of xylose was slower than the initial rate of APH of acetaldehyde and propanal (except for the 3 wt% Ru and all Co catalysts), indicating that the hydroxyl groups in xylose typically cause steric hindrance impeding the rate of xylose hydrogenation. The furan ring of furfural may also cause steric hindrance inhibiting the rate of furfural hydrogenation. The initial rate of aqueous-phase hydrogenolysis of THFA and xylitol was far slower than the initial rate of APH of the carbonyl groups even though these molecules were converted at much higher temperatures (523 K and 473 K respectively). Pt and Ni produced 1,2-pentanediol and 1,5-pentanediol respectively from aqueous-phase hydrogenolysis of THFA. Ru was the most active metal for C—C bond hydrogenolysis of xylitol.

Acknowledgements

This work was supported as part of the Catalysis Center for Energy Innovation, an Energy Frontier Research Center funded by the U.S. Department of Energy, Office of Science, Office of Basic Energy Sciences under Award Number DE-SC0001004. Theoretical work was performed at the Center for Nanophase Materials Sciences, which is sponsored at Oak Ridge National Laboratory by the Scientific User Facilities Division, Office of Basic Energy Sciences, U.S. Department of Energy, and used computing resources of the National Energy Research Scientific Computing Center, which is supported by US-DOE Office of Science under Contract DE-AC02-05CH11231.

Appendix A. Supplementary data

Supplementary data associated with this article can be found, in the online version, at http://dx.doi.org/10.1016/j.apcatb.2013.03.031.

References

[1] G.W. Huber, J.N. Chheda, C.J. Barrett, J.A. Dumesic, Science 308 (2005) 1446–1450.
[2] G.W. Huber, R.D. Cortright, J.A. Dumesic, Angewandte Chemie-International Edition 43 (2004) 1549–1551.
[3] J.N. Chheda, J.A. Dumesic, Catalysis Today 123 (2007) 59–70.
[4] R.R. Davda, J.W. Shabaker, G.W. Huber, R.D. Cortright, J.A. Dumesic, Applied Catalysis B 56 (2005) 171–186.
[5] G.W. Huber, J.A. Dumesic, Catalysis Today 111 (2006) 119–132.
[6] J.W. Shabaker, G.W. Huber, R.R. Davda, R.D. Cortright, J.A. Dumesic, Catalysis Letters 88 (2003) 1–8.
[7] T.P. Vispute, H.Y. Zhang, A. Sanna, R. Xiao, G.W. Huber, Science 330 (2010) 1222–1227.
[8] D.C. Elliott, Energy and Fuels 21 (2007) 1792–1815.
[9] M. Toba, Y. Abe, H. Kuramochi, M. Osako, T. Mochizuki, Y. Yoshimura, Catalysis Today 164 (2011) 533–537.
[10] O.V. Kikhtyanin, A.E. Rubanov, A.B. Ayupov, G.V. Echevsky, Fuel 89 (2010) 3085–3092.
[11] T.R. Brown, Y.N. Zhang, G.P. Hu, R.C. Brown, Biofuels, Bioproducts and Biorefining 6 (2012) 73–87.
[12] P.L. Dhepe, A. Fukuoka, ChemSusChem 1 (2008) 969–975.
[13] J.J. Bozell, G.R. Petersen, Green Chemistry 12 (2010) 539–554.
[14] G.W. Huber, S. Iborra, A. Corma, Chemical Reviews 106 (2006) 4044–4098.
[15] N. Li, G.A. Tompsett, G.W. Huber, ChemSusChem 3 (2010) 1154–1157.
[16] R.D. Cortright, M. Sanchez-Castillo, J.A. Dumesic, Applied Catalysis B 39 (2002) 353–359.
[17] Y.Q. Chen, D.J. Miller, J.E. Jackson, Industrial and Engineering Chemistry Research 46 (2007) 3334–3340.
[18] H. Olcay, L.J. Xu, Y. Xu, G.W. Huber, ChemCatChem 2 (2010) 1420–1424.
[19] H.L. Zhang, Y.Y. Yang, W. Dai, D. Yang, S.L. Lu, Y.Y. Ji, Catalysis Science and Technology 2 (2012) 1319–1323.
[20] J. Matos, A. Corma, Applied Catalysis A 404 (2011) 103–112.
[21] N.E. Musselwhite, S.B. Wagner, K.A. Manbeck, L.M. Carl, K.M. Gross, A.L. Marsh, Applied Catalysis A 402 (2011) 104–109.
[22] Y. Perez, M. Fajardo, A. Corma, Catalysis Communications 12 (2011) 1071–1074.
[23] J.A. Anderson, A. Athawale, F.E. Imrie, F.M. McKenna, A. McCue, D. Molyneux, K. Power, M. Shand, R.P.K. Wells, Journal of Catalysis 270 (2010) 9–15.
[24] A. Shukla, J.V. Pande, A. Bansiwal, P. Osiceanu, R.B. Biniwale, Catalysis Letters 131 (2009) 451–457.
[25] Y. Tang, S.J. Miao, H.N. Pham, A. Datye, X.M. Zheng, B.H. Shanks, Applied Catalysis A 406 (2011) 81–88.
[26] E.P. Maris, W.C. Ketchie, V. Oleshko, R.J. Davis, Journal of Physical Chemistry B 110 (2006) 7869–7876.
[27] S. Narayanan, R. Unnikrishnan, Journal of the Chemical Society, Faraday Transactions 94 (1998) 1123–1128.
[28] J. Wisniak, M. Hershkowitz, S. Stein, Industrial and Engineering Chemistry Product Research and Development 13 (1974) 232–236.
[29] B. Coq, F. Figueras, P. Geneste, C. Moreau, P. Moreau, M. Warawdekar, Journal of Molecular Catalysis 78 (1993) 211–226.
[30] G.W. Huber, J.W. Shabaker, S.T. Evans, J.A. Dumesic, Applied Catalysis B 62 (2006) 226–235.
[31] T.A. Manz, K.T. Thomson, J.M. Caruthers, W.N. Delgass, M.M. Abu-Omar, K. Phomphrai, S. Sharma, G. Medvedev, K.A. Novstrup, A.E. Fenwick, Abstracts of Papers of the American Chemical Society 235 (2008).
[32] R.J. Hendershot, S.S. Lasko, M.F. Fellmann, G. Oskarsdottir, W.N. Delgass, C.M. Snively, J. Lauterbach, Applied Catalysis A 254 (2003) 107–120.
[33] P. Serna, L.A. Baumes, M. Moliner, A. Corma, Journal of Catalysis 258 (2008) 25–34.
[34] L.A. Baumes, P. Serna, A. Corma, Applied Catalysis A 381 (2010) 197–208.
[35] U. Rodemerck, D. Wolf, O.V. Buyevskaya, P. Claus, S. Senkan, M. Baerns, Chemical Engineering Journal 82 (2001) 3–11.
[36] I. Onal, D. Duzenli, A. Seubsai, M. Kahn, E. Seker, S. Senkan, Topics in Catalysis 53 (2010) 92–99.
[37] J.E. Bedenbaugh, J. Ashok, A. Chien, S. Kim, S. Salim, M. Glascock, J. Lauterbach, Materials Research Society Symposium Proceedings 1425 (2012).
[38] G.W. Huber, J.W. Shabaker, J.A. Dumesic, Science 300 (2003) 2075–2077.
[39] Y.M. Liu, P.J. Cong, R.D. Doolen, S.H. Guan, V. Markov, L. Woo, S. Zeyss, U. Dingerdissen, Applied Catalysis A 254 (2003) 59–66.
[40] J. Greeley, T.F. Jaramillo, J. Bonde, I.B. Chorkendorff, J.K. Norskov, Nature Materials 5 (2006) 909–913.
[41] P. Maki-Arvela, L.P. Tiainen, M. Lindblad, K. Demirkan, N. Kumar, R. Sjoholm, T. Ollonqvist, J. Vayrynen, T. Salmi, D.Y. Murzin, Applied Catalysis A 241 (2003) 271–288.
[42] B. Echchahed, S. Kaliaguine, H.S. Alamdari, International Journal of Chemical Reactor Engineering 4 (2006).
[43] X. Shen, L.J. Garces, Y. Ding, K. Laubernds, R.P. Zerger, M. Aindow, E.J. Neth, S.L. Suib, Applied Catalysis A 335 (2008) 187–195.
[44] A. Corma, J.M. Serra, A. Chica, Catalysis Today 81 (2003) 495–506.
[45] S. Senkan, K. Krantz, S. Ozturk, V. Zengin, I. Onal, Angewandte Chemie-International Edition 38 (1999) 2794–2799.
[46] J.W. Saalfrank, W.F. Maier, Angewandte Chemie-International Edition 43 (2004) 2028–2031.
[47] P. Desrosiers, S.H. Guan, A. Hagemeyer, D.M. Lowe, C. Lugmair, D.M. Poojary, H. Turner, H. Weinberg, X.P. Zhou, R. Armbrust, G. Fengler, U. Notheis, Catalysis Today 81 (2003) 319–328.
[48] R. Vijay, R.J. Hendershot, S.M. Rivera-Jimenez, W.B. Rogers, B.J. Feist, C.M. Snively, J. Lauterbach, Catalysis Communications 6 (2005) 167–171.
[49] C. Kiener, M. Kurtz, H. Wilmer, C. Hoffmann, H.W. Schmidt, J.D. Grunwaldt, M. Muhler, F. Schuth, Journal of Catalysis 216 (2003) 110–119.

[50] J.P. Perdew, K. Burke, M. Ernzerhof, Physical Review Letters 77 (1996) 3865–3868.
[51] G. Kresse, J. Hafner, Physical Review B 49 (1994) 14251–14269.
[52] G. Kresse, J. Furthmuller, Computation Materials Science 6 (1996) 15–50.
[53] G. Kresse, J. Furthmuller, Physical Review B 54 (1996) 11169–11186.
[54] G. Kresse, D. Joubert, Physical Review B 59 (1999) 1758–1775.
[55] N.W. Ashcroft, N.D. Mermin, Solid State Physics, Saunders College, Orlando, FL (1976).
[56] J. Neugebauer, M. Scheffler, Physical Review B 46 (1992) 16067–16080.
[57] C.H. Bartholomew, in: C.H. Bartholomew, G.A. Fuentes (Eds.) Studies in Surface Science and Catalysis, Elsevier (1997) 585–592.
[58] X. Wang, N. Perret, M.A. Keane, Chemical Engineering Journal 210 (2012) 103–113.
[59] G. Ertl, H. Knözinger, F. Schüth, J. Weiktamp (Eds.), Handbook of Heterogeneous Catalysis, 2nd ed., Wiley-VCH, Weinheim, 2008.
[60] J. Wisniak, M. Hershkow, R. Leibowit, S. Stein, Industrial and Engineering Chemistry Product Research and Development 13 (1974) 75–79.
[61] M. Yadav, D.K. Mishra, J.-S. Hwang, Applied Catalysis A 425–426 (2012) 110–116.
[62] R.Y. Zheng, Y.X. Zhu, J.G.G. Chen, ChemCatChem 3 (2011) 578–581.
[63] G.M.R. van Druten, V. Ponec, Applied Catalysis A 191 (2000) 153–162.
[64] S. Sitthisa, D.E. Resasco, Catalysis Letters 141 (2011) 784–791.
[65] N. Li, G.W. Huber, Journal of Catalysis 270 (2010) 48–59.
[66] J.Y. Sun, H.C. Liu, Green Chemistry 13 (2011) 135–142.
[67] E.P. Maris, R.J. Davis, Journal of Catalysis 249 (2007) 328–337.
[68] R.R. Davda, J.W. Shabaker, G.W. Huber, R.D. Cortright, J.A. Dumesic, Applied Catalysis B 43 (2003) 13–26.
[69] D.E. Resasco, S. Sitthisa, J. Faria, T. Prasomsri, M.P. Ruiz, in: D. Kubička, I. Kubičková (Eds.), Heterogeneous Catalysis in Biomass to Chemicals and Fuels, Research Signpost, Trivandrum, 2011, pp. 155–188.
[70] W.J. Yu, Y. Tang, L.Y. Mo, P. Chen, H. Lou, X.M. Zheng, Bioresource Technology 102 (2011) 8241–8246.
[71] J. Tobicik, L. Cerveny, Journal of Molecular Catalysis A: Chemical 194 (2003) 249–254.
[72] R.M. Ravenelle, J.R. Copeland, W.G. Kim, J.C. Crittenden, C. Sievers, ACS Catalysis 1 (2011) 552–561.
[73] H.T. Li, Y.X. Zhao, C.G. Gao, Y.Z. Wang, Z.J. Sun, X.Y. Liang, Chemical Engineering Journal 181 (2012) 501–507.
[74] J.W. Shabaker, G.W. Huber, J.A. Dumesic, Journal of Catalysis 222 (2004) 180–191.
[75] C.H. Bartholomew, Applied Catalysis A 107 (1993) 1–57.
[76] D.C. Elliott, Abstracts of Papers of the American Chemical Society 223 (2002).
[77] C.H. Bartholomew, R.J. Farrauto, Fundamentals of Industrial Catalytic Processes, 2nd ed., John Wiley & Sons, Inc., Hoboken, NJ, 2005.
[78] F. Abild-Pedersen, J. Greeley, F. Studt, J. Rossmeisl, T.R. Munter, P.G. Moses, E. Skulason, T. Bligaard, J.K. Norskov, Physical Review Letters 99 (2007) 016105.
[79] P. Ferrin, D. Simonetti, S. Kandoi, E. Kunkes, J.A. Dumesic, J.K. Norskov, M. Mavrikakis, Journal of the American Chemical Society 131 (2009) 5809–5815.
[80] S. Dahl, A. Logadottir, R.C. Egeberg, J.H. Larsen, I. Chorkendorff, E. Tornqvist, J.K. Norskov, Physical Review Letters 83 (1999) 1814–1817.
[81] T. Zambelli, J. Wintterlin, J. Trost, G. Ertl, Science 273 (1996) 1688–1690.
[82] M.P. Andersson, E. Abild-Pedersen, I.N. Remediakis, T. Bligaard, G. Jones, J. Engbwk, O. Lytken, S. Horch, J.H. Nielsen, J. Sehested, J.R. Rostrup-Nielsen, J.K. Norskov, I. Chorkendorff, Journal of Catalysis 255 (2008) 6–19.
[83] R.T. Vang, K. Honkala, S. Dahl, E.K. Vestergaard, J. Schnadt, E. Laegsgaard, B.S. Clausen, J.K. Norskov, F. Besenbacher, Nature Materials 4 (2005) 160–162.
[84] L.J. Xu, Y. Xu, Catalysis Today 165 (2011) 96–105.
[85] A.C. Lausche, J.S. Hummelshoj, F. Abild-Pedersen, F. Studt, J.K. Norskov, Journal of Catalysis 291 (2012) 133–137.
[86] S.H. Pang, A.M. Roman, J.W. Medlin, Journal of Physical Chemistry C 116 (2012) 13654–13660.